

Satellite observations of Antarctic sea ice thickness and volume

Nathan Kurtz^{1,2}, Thorsten Markus²

¹Goddard Earth Sciences Technology and Research, Morgan State University, Baltimore,
MD 21251

²Hydrospheric and Biospheric Sciences Laboratory, NASA Goddard Space Flight Center,
Greenbelt, MD 20771

Abstract

We utilize satellite laser altimetry data from ICESat combined with passive microwave measurements to analyze basin-wide changes in Antarctic sea ice thickness and volume over a 5 year period from 2003-2008. Sea ice thickness exhibits a small negative trend while area increases in the summer and fall balanced losses in thickness leading to small overall volume changes. Using a five year time-series, we show that only small ice thickness changes of less than $-0.03 \frac{m}{yr}$ and volume changes of $-266 \frac{km^3}{yr}$ and $160 \frac{km^3}{yr}$ occurred for the spring and summer periods, respectively. The calculated thickness and volume trends are small compared to the observational time period and interannual variability which masks the determination of long-term trend or cyclical variability in the sea ice cover. These results are in stark contrast to the much greater observed losses in Arctic sea ice volume and illustrate the different hemispheric changes of the polar sea ice covers in recent years.

1 Introduction

The Earth's sea ice cover greatly influences the global climate by reflecting a large portion of the incoming solar radiation and providing a strongly insulating layer between the ocean and atmosphere. The annual cycle of sea ice growth and decay affects oceanic salinity which influences deep water formation and circulation of the world ocean (*Gordon, 1991*). Recent observations of large losses of Arctic sea ice are considered a key indicator of changes presently occurring in the climate (e.g. *Comiso et al., 2008; Stroeve et al., 2007; Giles et al., 2008; Kwok et al., 2009; Kurtz et al., 2011; Screen and Simmonds, 2010*). However, large-scale observations of Antarctic sea ice thickness and volume are still missing in order to determine trends and assess predictive models of future global climate change (*Lemke et al., 2007*).

In contrast to declining Arctic sea ice, some models show the overall volume of the Antarctic sea ice cover may increase under a warming climate (*Zhang, 2007; Powell et al., 2005*), while those used in global climate models predict a decrease (*Gupta et al., 2009; Liu and Curry, 2010*). Furthermore, model simulations also predict that increased global temperatures may lead to increased precipitation over the Southern Ocean (*Watterson and Dix, 2003*), these changes in precipitation may lead to substantial changes in the thickness and volume of ice in the Southern Ocean through reduction of the oceanic convective heat flux (*Manabe, 1992*). However, observational data of sea ice thickness and volume data across the Antarctic basin are still critically needed to support these hypotheses and more fully understand the impact of changes currently occurring in the polar climate systems.

Much of our current knowledge of Antarctic sea ice comes from satellite passive microwave measurements which have shown a slight increase in the areal coverage of sea ice over the last three decades (*Zwally et al., 2002*). More recently, satellite altimetry data have been applied to the study of Antarctic sea ice. The use of satellite radar altimetry data for the potential study of Antarctic sea ice thickness has been investigated, while the results show

some promise, the results are complicated by the fact that the radar signal may be reflected from an undetermined point within the snow layer rather than the snow-air or snow-ice interface (*Giles et al.*, 2008; *Willatt et al.*, 2010). Penetration of an infrared laser pulse into the snow layer is small, thus laser altimetry data are a promising way to study the Antarctic sea ice cover irrespective of the complicated snow morphology that is often found (*Massom et al.*, 2001). *Zwally et al.*, [2008] and *Yi et al.*, [2011] used a combination of satellite laser altimetry data from NASA’s Ice, Cloud, and land Elevation Satellite (ICESat) with snow depth retrievals from passive microwave data to estimate sea ice thickness in the Weddell Sea. They found a near zero trend in ice volume in the area suggesting that the large losses in multiyear sea ice thickness seen in the Arctic may not be present in the Antarctic. These and other studies (e.g. *Weissling and Ackley*, 2011; *Xie et al.*, 2011) have demonstrated the potential of satellite laser altimetry data to be used in the retrieval of sea ice thickness, but to date this has not been done for the whole of the Antarctic basin. In this study, we utilize satellite laser and passive microwave data to provide a first time estimate of basin-wide Antarctic sea ice volume and the changes which occurred over a 5 year period spanning the lifetime of NASA’s Ice, Cloud, and land Elevation Satellite (ICESat).

The study is organized as follows. A description of the data sets is presented in Section 2. The methodology for the retrieval of sea ice thickness and volume is described in Section 3. Comparisons of the satellite derived thickness data with in-situ measurements are described in Section 4. Section 5 presents the regional to basin-wide observations and trends. The results of the study are summarized in Section 6.

2 Data sets

ICESat sea ice elevation data products (*Zwally et al.* 2003) were used as the starting point to determine the sea ice freeboard. Here, we refer to sea ice freeboard as the height of the

ice plus snow layers above the water level as this is what is measured by the laser altimeter aboard ICESat. The ICESat data have a footprint size of ~ 70 m and a shot-to-shot spacing of 172 m. ICESat data were limited to the 13 campaign periods shown in Table 1, our analysis is thus restricted to these time periods when ICESat data is available.

We first filtered out ICESat elevation data which have been significantly affected by atmospheric scattering such as from clouds or blowing snow. Scattering events increase the path length traveled by the photons which biases the retrieved elevation. These biased elevation data are identified from instrument and waveform derived parameters and removed using similar, but more conservative filtering parameters described by *Zwally et al.* [2008]. Specifically (1) data with a detector gain (*i_gval_rcv* in the GLA13 product) greater than 30 counts (60 counts for the low energy MJ04 campaign) are removed due to the high probability of being affected by atmospheric scattering and having a low signal-to-noise ratio (SNR); (2) data with a difference between the received waveform and fitted Gaussian (*i_SeaIceVar*) greater than 80 millivolts may be significantly affected by atmospheric scattering and are removed; and (3) data with a reflectivity (uncorrected for atmospheric effects, *i_reflectUncorr*) less than 0.05 (indicating a low signal) and greater than 1 (indicating a heavily saturated waveform) are removed; (4) data with a maximum received pulse amplitude (*i_maxSmAmp*) less than 0.4 volts for high energy campaigns (ON03 and ON04) and 0.3 volts for all other campaigns are also removed.

The areal coverage of sea ice was obtained from Special Sensor Microwave Imager (SSM/I) data using the NASA Team 2 algorithm (*Markus and Cavalieri, 2000*) to discriminate between the sea ice pack and open ocean. ICESat freeboard retrievals were only done in areas within the main sea ice pack and extending northwards towards the marginal sea ice zone where the ice areal coverage (ice concentration) was greater than 50%. This was done to reduce the impact of ocean waves which can bias the retrieved freeboard (*Zwally et al., 2008*).

3 Methodology of sea ice thickness and volume retrievals

Our approach to determine the thickness and volume of the sea ice cover follows from the retrieval of sea ice freeboard from ICESat following the procedure described in *Markus et al.*, [2011] and an assumption of hydrostatic balance to determine the total thickness of the sea ice above and below the water level. The freeboard retrieval method used here selectively identifies reference sea surface elevations within the ICESat data set, which when subtracted from the sea ice elevation data, yields the height of the snow plus sea ice layers above the water level termed the sea ice freeboard. The hydrostatic balance equation is used to infer the sea ice thickness from the retrieved sea ice freeboard values through observational estimates of the densities of snow, ice, and water.

Assuming hydrostatic balance, the total sea ice thickness above and below the water line, h_i , is found using the following equation

$$h_i = \frac{\rho_s - \rho_w}{\rho_w - \rho_i} h_s + \frac{\rho_w}{\rho_w - \rho_i} h_f \quad (1)$$

where h_s is the snow depth, h_f the freeboard (defined here as the height of the sea ice plus snow layers above sea level), ρ_s , ρ_i , and ρ_w are the densities of snow, sea ice, and sea water, respectively. ICESat sea ice elevation data products are used to determine the sea ice freeboard where local sea surface reference points are identified. Sea ice freeboard can be found from ICESat elevation data, h_e , by subtracting the local sea surface height, h_{ssh}

$$h_f = h_e - h_{ssh}$$

An initial estimate for h_{ssh} was first made by summing the contributions of the geoid, tides, and atmospheric pressure variations at each ICESat measurement and subtracting it from h_e . Sea surface tiepoints were identified within the data where the elevation is below an

expected deviation from the local mean surface. Sea ice freeboard was retrieved for each available elevation measurement where a suitable sea surface tiepoint was available within 12.5 km.

Using equation 1, sea ice freeboard can be converted into an ice thickness value through knowledge of the snow depth and densities of snow, sea ice, and sea water. In this study, the density of sea water is taken to be $\rho_w = 1024 \frac{kg}{m^3}$ (*Fichefet and Morales-Maqueda*, 1999). The snow density is taken to be seasonally varying with values of $\rho_s = 320 \frac{kg}{m^3}$, $\rho_s = 350 \frac{kg}{m^3}$, and $\rho_s = 340 \frac{kg}{m^3}$ for the spring, summer, and fall periods respectively. These values were estimated by averaging the density values for a number of ship cruises summarized by *Massom et al.*, 2001. The sea ice density is also taken to be seasonally varying at $\rho_i = 900 \frac{kg}{m^3}$ for the spring and fall periods and $\rho_i = 875 \frac{kg}{m^3}$ for the summer period following *Worby et al.*, [2008] and the observations of *Buynitskiy*, [1967].

Accounting for snow loading in the ice thickness retrievals is much more difficult because of the large uncertainties present in available snow depth data sets. We address the issue of snow loading through an error analysis approach in order to determine the optimal method for estimating the snow loading contribution in a way which minimizes the expected errors in the retrieved ice thickness values. Excluding the negligible contribution of errors due to variations in sea water density (*Kwok and Cunningham*, 2008), the error in the ice thickness retrieval (equation 1) is

$$\sigma_{h_i} = \left[\left(\frac{\rho_w}{\rho_w - \rho_i} \right)^2 \sigma_{h_f}^2 + \left(\frac{\rho_s - \rho_w}{\rho_w - \rho_i} \right)^2 \sigma_{h_s}^2 + \left(\frac{h_s(\rho_s - \rho_w) + h_f \rho_w}{(\rho_w - \rho_i)^2} \right)^2 \sigma_{\rho_i}^2 + \left(\frac{h_s}{\rho_w - \rho_i} \right)^2 \sigma_{\rho_s}^2 \right]^{\frac{1}{2}} \quad (2)$$

where σ_{h_i} , σ_{h_f} , σ_{h_s} , σ_{ρ_s} , and σ_{ρ_i} are the uncertainties of the ice thickness, freeboard, snow depth, and densities of snow and ice, respectively. Following the detailed discussion in *Maksym and Markus*, [2008], we use estimates of $\sigma_{\rho_i} = 20 \frac{kg}{m^3}$ for the sea ice density

uncertainty and $\sigma_{\rho_s} = 50 \frac{kg}{m^3}$ for the snow density uncertainty. The estimated σ_{h_f} for the ICESat freeboard retrieval method is 1.8 cm (*Markus et al.*, 2011). This comparison took place over an area spanning 50 km by 100 km and is an estimate of the uncertainty of the ICESat data on a local scale. Given this small uncertainty on the local scale, we estimate that over a regional to basin scale the random error in the freeboard data reduces to zero given the large number of measurements taken.

Uncertainties in the ice thickness due to snow depth errors will depend greatly on the choice of available snow depth estimates which currently include either passive microwave or model approaches. Passive microwave snow depth retrieval methods (*Markus and Cavalieri*, 1998) have an estimated uncertainty of 5 cm and a bias of ~ 3.5 cm with higher regional differences also seen (*Massom et al.*, 2006). Snow depth from reanalysis precipitation estimates have been used in the Arctic region (*Kwok and Cunningham*, 2008) and could similarly be applied to the Antarctic region, but artifacts and errors in these data sets are still problematic (*Nicolas and Bromwich*, 2011). An error of at least 5 cm has been estimated for snow depth derived from model data for the Arctic region (*Kwok and Cunningham*, 2008). For the Antarctic region, it has been shown that approximately half of the precipitating snow cover is lost to open water leads which would greatly bias the use of snow models from precipitation data alone (*Leonard and Maksym*, 2011). However, in-situ observations have shown it is reasonable to assume that over the scale of an ice floe the height of the sea ice layer above the water level (ice freeboard), fb , is near zero (*Adolphs*, 1998; *Jeffries et al.*, 1998; *Weissling and Ackley*, 2011). Another recent study by *Xie et al.*, [2011] showed specifically that the zero ice freeboard assumption was applicable to determine sea ice thickness from ICESat data in the Bellingshausen Sea region. Using this assumption of zero ice freeboard the freeboard measurements from ICESat are equivalent to the snow depth, h_s . This allows the ICESat data to be used in the calculation of the ice thickness through the previously described parameters without the need for a snow depth data set. In this situation, the error

in ice thickness can be written as

$$\sigma_{h_i} = \left[\frac{\sigma_{\rho_s}^2 h_s^2 + \sigma_{fb}^2 \rho_w^2}{(\rho_w - \rho_i)^2} + \frac{\sigma_{\rho_i}^2 \rho_s^2 h_s^2}{(\rho_w - \rho_i)^4} \right]^{\frac{1}{2}} \quad (3)$$

where σ_{fb} is the error in the ice freeboard. Estimates of the mean value of fb for the Antarctic basin from analyses of both passive microwave and in-situ data sets is ~ 1 cm (*Maksym and Markus, 2008*). As a conservative estimate we take σ_{fb} to be 2 cm for the purposes of our error analysis. From equation 3 and the ICESat freeboards calculated over the Antarctic basin we estimate an overall ice thickness error of 23 cm using the assumption of zero ice freeboard. Using the same snow depth and freeboard values but considering an error in snow depth to be 5 cm (e.g. expected from passive microwave snow depth retrievals) and equation 2, we find a higher error of 37 cm in ice thickness. Overall, we find that as long as σ_{fb} is less than ~ 4 cm the zero freeboard assumption will give a result with the lowest uncertainty and is thus the optimum choice for the ice thickness retrievals used in this study. While the value reported using the zero freeboard assumption gives the lower bound in ice thickness and the accuracy may vary regionally (*Worby et al., 2011*), it nonetheless should be a useful estimate of the mean ice thickness over the Antarctic basin and for determining ice thickness and volume trends.

To determine the average sea ice thickness and volume for the Antarctic basin, the high resolution ICESat freeboard data were first gridded onto a 25 km polar stereographic projection grid. A 25 km grid size is used to coincide with the expected scale at which the sampling error of the ICESat data set is minimized (*Weissling and Ackley, 2011*). Using the assumption of zero ice freeboard, sea ice thickness was calculated for each grid cell through a modification to equation 1 as

$$h_i^n = \frac{\rho_s}{\rho_w - \rho_i} h_f^n$$

where h_i^n and h_f^n are the sea ice thickness and sea ice freeboard of each 25 km grid cell, n . For each grid cell, we then fill in gaps in the gridded data using a distance weighted Gaussian function as follows

$$h_i^n = \sum_j^N w_j h_i^j$$

where w_j is the normalized weight which is calculated as

$$w_j = \exp\left(\frac{d_{jn}}{c}\right)$$

where d_{jn} is the distance between grid cells j and n , and c is the correlation length scale taken to be 125 km (*Worby et al.*, 2008).

The volume of the sea ice cover was calculated by multiplying the area of each grid cell by the mean retrieved ICESat sea ice thickness value within the grid cell. The locations of sea ice covered grid cells were determined from Special Sensor Microwave Imager (SSM/I) satellite data using the NASA Team 2 algorithm (*Markus and Cavalieri*, 2000). Combined sea ice thickness and volume fields were retrieved over the sea ice area (excluding the marginal sea ice zone towards the ice edge where ice areal coverage was less than 50%) using five years of ICESat data to analyze the changes and variability in the sea ice cover which took place over the 2003-2008 time period.

The overall ice thickness uncertainty of 23 cm applies to the absolute determination of the mean sea ice thickness. For the purpose of determining trends in the sea ice thickness and volume, the uncertainty is dependent on the interannual variability of the density terms. If the retrieval method is unbiased and the interannual variability of the sea ice and snow densities is small, then the uncertainty for the basinwide mean sea ice thickness is

$$\langle \sigma_{h_i} \rangle = \frac{\sigma_{h_i}}{\sqrt{N}}$$

where N is the number of grid cells. Similarly, the uncertainty in the mean sea ice volume, σ_{vol} is

$$\langle \sigma_{vol} \rangle = \frac{\left(A^2 \langle \sigma_{h_i}^2 \rangle + h_i^2 \sigma_A^2 \right)^{1/2}}{\sqrt{N}}$$

where A is the sea ice areal coverage and σ_A is the uncertainty in the sea ice areal coverage. N varies from a minimum of $\sim 5,000$ in the summer time to a maximum of $\sim 30,000$ in the spring. Due to the large number of observations taken, the uncertainties in mean sea ice thickness and total volume are expected to be small. However, this should be regarded as the best case scenario, if there is interannual variability in the density of sea ice and snow then these terms will introduce additional uncertainty in the mean thickness and volume trends.

4 Comparisons with ship-based observations

To investigate the reliability of sea ice thickness data from the ICESat data set, we compare our data with ship-based observations from the Antarctic Sea Ice Processes and Climate (ASPeCt) data set. Since ICESat measures both undeformed and deformed ice, we compare the ICESat values with the ASPeCt average ice thickness which incorporates the contributions of ridged and level ice. The ASPeCt ice thickness data are comprised of 81 cruises into the Antarctic ice pack between 1981 and 2005, observations within 6 nautical miles of the previous observation have been removed to avoid sampling biases. Errors in the ASPeCt thickness are

estimated to range from $\pm 20\%$ for level ice greater than 0.3 m to up to $\pm 50\%$ for ridged ice (Worby *et al.*, 2008).

In order to place the ASPeCt observations onto the same seasonal and spatial scales as the ICESat data, we have placed the ASPeCt observations onto the same 25 km polar stereographic grid as ICESat. Table 2 shows the comparison between the data sets for two time periods: 1) All ship-based observations for each respective season from the 1981-2005 period have been averaged to provide an estimation of a climatological data set. To minimize time discrepancies between the climatological data and the ICESat measurements, the measurements were averaged only within the same months of the ICESat campaigns shown in Table 1. 2) All ship-based observations that occurred during the ICESat measurement periods have also been averaged to provide a more temporally limited comparison by season. There were no fall ASPeCt measurements within the same data collection time period as the ICESat data campaigns so no comparison for these times was possible.

The spring season compared most favorably to the ASPeCt thickness data with mean differences of 4 cm and 6 cm for observations over the 1981-2005 time period and 2003-2005 time periods, respectively. Clear seasonal differences can be seen for the summer time periods with differences of 16 cm and 23 cm between the observation time periods. Overall, there appears to be good general agreement between the ICESat and ASPeCt data sets with mean differences of 10 cm for the climatological data set and 15 cm for the time coincident data set. The mean thickness values for both the climatological and direct comparison are within the estimated $\pm 1\sigma$ uncertainty of the ICESat derived thicknesses estimated previously. Additionally, the mean ICESat thickness values are all greater than the corresponding ASPeCt values. If the assumption of zero freeboard were not a reasonable assumption we would expect the opposite to occur with ICESat showing lower thickness values. The overall good agreement lends confidence in the validity of the measurements and assumptions used to calculate sea ice thickness from the ICESat data.

5 Sea ice thickness and volume results

Maps of the seasonally averaged sea ice thickness values are shown in Figure 1. Figure 1 shows that the thickest ice resides in the western Weddell Sea, the Bellingshausen and Amundsen Seas, the western Ross sea, and surrounding the Antarctic coastline. The thinnest ice is found in the eastern Weddell Sea, the Ross Sea, portions of the Indian and Pacific Oceans, and towards the northern edge of the sea ice cover. Seasonal differences in the data can also be seen with primarily the areas containing thick ice surviving into the summer melt season. During the fall, large areas of thin ice were observed in the eastern Weddell Sea and expanding outward towards the ice edge. The absence of a gradient towards zero ice thickness in some areas of the ice edge is due to the requirement of at least 50% sea ice areal coverage within the gridded thickness fields. In the spring season, an expansion of the thick ice areas in the Weddell Sea was observed along with large areas of thin, young ice. The spatial and temporal distributions of sea ice thickness observed by ICESat are also broadly consistent with the ship-based climatological compilation of *Worby et al.*, [2008].

Figure 3 shows the averaged freeboard and thickness values for the Southern Ocean for all of the ICESat operational time periods. Also shown are the ice areal coverage taken from the SSM/I data and the subsequent ice volume. The total volume of ice varies substantially over the annual cycle due mainly to the large annual growth cycle and associated changes of ice extent. The ICESat record shows the 2003-2008 mean ice volume reached a minimum of 3357 km^3 in the summer, grew to 8125 km^3 in the fall, and reached its maximum of 11111 km^3 in the spring. Thus, the amplitude in the annual cycle of ice production and melt (less ice export) was $\sim 8000 \text{ km}^3$. This annual cycle of ice production and melt is larger than that of the Arctic which has an annual ice production of $\sim 3400 \text{ km}^3$, though a higher maximum ice volume of 16400 km^3 in the spring (*Kwok et al.*, 2009).

The distribution of the sea thickness measurements are shown in Figure 2. The mode of

the thickness distributions for the spring and fall seasons is between 20 and 30 cm for all seasons. This is also around the maximum thickness that the pack ice has been observed to thermodynamically grow before it is deformed (*Allison and Worby, 1994; Jeffries et al., 1997; Wadhams et al., 1987*) suggesting that undeformed ice is the most frequent sea ice type Antarctic. The large tails of the distributions and mean thickness values of > 70 cm suggest that much of the ice volume is from deformed ice.

Trends in the mean sea ice thickness and volume over the five year time period are shown in Table 3. ICESat data were limited to the times shown in Table 1, our analysis is thus restricted to these time periods when ICESat data is available. A difficulty in discerning trends in the data is due to the fact that the ICESat operational periods do not always start and end on the same dates. This causes additional variability in the data sets and complicates interpretation of the true annual trends in sea ice volume. This impact was found to be of greatest importance in the 2005 and 2006 spring ICESat campaigns which began almost 3 weeks later than those for the previous spring campaigns. Thus, melting of the ice had already begun in some regions which decreased the ice area and thus ice volume observed in our data set. To quantify the impact of these differences for the trend calculations, we calculate two separate trends in ice area and volume: 1) using the specified time periods in Table 1, and 2) using ice areal coverage for the spring 2005 and 2006 campaigns with dates equivalent to the spring 2004 data set. In the following we discuss the thickness trends with respect to case 2), as melting of the ice distorts the calculated trend in volume loss for case 1) due to the natural temporal cycle of ice melt.

In contrast to the large negative sea ice thickness trends of -0.2 m/yr recently observed in the Arctic (*Kwok et al., 2009*), we observed only small negative trends of less than -0.03 m/yr in the thickness of the Antarctic sea ice cover. The summer period shows the largest variability and negative trend of $-0.03 \frac{m}{yr}$ in the sea ice thickness data. Despite the negative thickness trend, the overall volume trend in the summer is positive at $160 \frac{km^3}{yr}$ ($4.8\% yr^{-1}$).

The spring period also showed small negative trends of $-0.02 \frac{m}{yr}$ in mean ice thickness. The volume trend for the spring period is negative at $-266 \frac{km^3}{yr}$ ($-2.4\% yr^{-1}$) due mainly to the loss of ice thickness rather than areal coverage of sea ice. This loss in sea ice volume is much smaller than the $-862 \frac{km^3}{yr}$ volume trend which has been observed for the late winter/early spring period in the Arctic (*Kwok et al.*, 2009).

To investigate regional trends in the data we divide the Antarctic into six longitudinally distinct regions following *Worby et al.*, [2008] and shown in Figure 4. The regional trends in Antarctic sea ice thickness and volume are shown in Table 3. With the exception of the Bellingshausen and Amundsen Seas, the summer time period exhibited negative thickness trends in all regions. These negative thickness trends were most prominent in the perennial ice area of the western Weddell Sea and the thick ice near the coast in the Indian Ocean sector. The Weddell Sea also showed negative ice thickness trends in the spring period as well. But losses of ice thickness in the Weddell Sea and other areas were found to be nearly balanced by large positive thickness trends in the Bellingshausen and Amundsen Seas, leading to only a slight negative trend in the overall mean ice thickness. For the summer periods, volume loss in the Bellingshausen, Amundsen, and western Weddell seas was mostly offset by volume gains in the Ross and eastern Weddell seas. These volume gains were due to increases in ice area, as the mean ice thickness decreased in all regions. The overall loss of ice volume in the spring was found to be due to losses in the mean ice thickness.

6 Summary

We have utilized satellite laser altimetry data from ICESat and passive microwave data from SSM/I to provide a first time estimate of both sea ice thickness and volume over the Southern Ocean. These observations are an important component of understanding past, present, and future changes to the Antarctic sea ice cover. Knowledge of Antarctic sea ice thickness and

volume is required for a diverse array of climate studies including global temperature changes (*Rind et al.*, 1997), sustainability of algae communities in the Southern Ocean ecosystem (e.g. *McMinn et al.*, 1999), assessing the representation of sea ice in global climate models, and many more.

An absolute uncertainty of 23 cm is calculated for our sea ice thickness results using a propagation of uncertainties in the input parameters to the hydrostatic balance equation. Agreement between our retrieved ICESat sea ice thickness values with in-situ data are all within the estimated uncertainty demonstrating the consistency of the retrieved ice thickness results. The extent to which long-term trends in the thickness and volume of the Antarctic sea ice cover can be found is limited due to the 5 year operational lifetime of the ICESat mission, as well as the limited temporal sampling. But linking these measurements to current and future airborne (e.g. NASA's Operation IceBridge) and satellite missions (e.g. ESA's CryoSat-2) will provide a vital component for understanding long-term changes in Antarctic sea ice and its impact on the climate. The statistical significance of the trends in sea ice thickness and volume depends primarily on the interannual variability of the densities of snow and ice, if the mean densities vary little on a year-to-year basis then the small trends calculated, while small, are still statistically significant. Determination of the interannual variability of the sea ice and snow density values thus remains a necessary component to fully assess trends in the sea ice thickness and volume from the satellite altimetry record.

The recent losses in Arctic sea ice volume are due predominantly to thinning and loss of the perennial sea ice cover (*Kwok et al.*, 2009). Similarly, we find that the recent volume losses in the spring for the Antarctic sea ice cover are also due to thinning of the sea ice, but this thinning is much smaller than that observed for the Arctic over the same 2003-2008 time period. Unlike the Arctic where the observed thinning is likely driven by thermodynamic and dynamic changes, the Antarctic sea ice variations could be driven more by precipitation changes which impact snow-ice formation and oceanic heat exchange. However, future work

with model simulations is needed to better understand the forcing factors which most heavily drive changes in the Southern Ocean sea ice cover.

7 References

Adolphs, U. Ice thickness variability, isostatic balance and potential for snow ice formation on ice floes in the south polar Pacific Ocean, *J. Geophys. Res.*, **103**, 24,675-24,691, 1998.

Allison, I., A. P. Worby, Seasonal changes of sea-ice characteristics off East Antarctica, *Ann. Glaciol.*, **20**, 195-201, 1994.

Buynitskiy, V. K. Structure, principal properties and strength of Antarctic sea ice, *Sov. Antarct. Exped. Inf. Bull., Engl. Transl.*, **65**, 504-510, 1967.

Comiso, J. C., Parkinson, C. L., Gersten, R. & Stock, L. Accelerated decline in the Arctic sea ice cover, *Geophys. Res. Lett.*, **35**, L01703, doi:10.1029/2007GL031972, 2008.

Fichefet, T., and M. A. Morales Maqueda, Modelling the influence of snow accumulation and snow-ice formation on the seasonal cycle of the Antarctic sea-ice cover, *Clim. Dyn.*, **15**, 251 – 268, 1999.

Giles, K. A., Laxon, S. W. & Ridout, A. L. Circumpolar thinning of Arctic sea ice following the 2007 record ice extent minimum, *Geophys. Res. Lett.*, **35**, L22502, doi:10.1029/2008GL035710, 2008.

Giles, K. A., Laxon, S. W. & Worby, A. P. Antarctic sea ice elevation from satellite radar altimetry, *Geophys. Res. Lett.*, **35**, L03503, doi:10.1029/2007GL031572, 2008.

Gordon, A. L. in *Deep Convection and Deep Water Formation in the Oceans*, Chu, P. C., Gascard, J. C. Eds. (Elsevier, New York, 1991).

Gupta, A. S., A. Santoso, A. S. Taschetto, C. C. Ummenhofer, J. Trevena, M. H. England, Projected changes to the southern hemisphere ocean and sea ice in the IPCC AR4 climate models, *J. Clim.*, **22**, 3047-3078, 2009.

Jeffries, M. O., A. P. Worby, K. Morris, W. F. Weeks, Seasonal variations in the properties and structural composition of sea ice and snow cover in the Bellingshausen and Amundsen Seas, Antarctic, *J. Glaciol.*, **43**(143), 138-151, 1997.

Jeffries, M. O., Li, S., Jana, R. A., Krouse, H. R. & Hurst-Cushing, B. Late winter first-year ice floe thickness variability, seawater flooding and snow ice formation in the Amundsen and Ross Seas, in Antarctic Sea Ice: Physical Processes, Interactions and Variability, in *Antarct. Res. Ser.*, **74**, 69-87, AGU, Washington D.C., 1998.

Kurtz, N. T., Markus, T., Farrell, S. L., Worthen, D. L. & Boisvert, L. N. Observations of recent Arctic sea ice volume loss and its impact on ocean-atmosphere energy exchange and ice production, *J. Geophys. Res.*, **116**, C04015, doi:10.1029/2010JC006235, 2011.

Kwok, R. & Cunningham, G. F. ICESat over Arctic sea ice: Estimation of snow depth and ice thickness, *J. Geophys. Res.*, **113**, C08010, 2008.

Kwok, R., G.F. Cunningham, M. Wensnahan, I. Rigor, H.J. Zwally, and D. Yi, Thinning and volume loss of the Arctic Ocean sea ice cover: 2003-2008, *J. Geophys. Res.*, **114**, C07005, doi:10.1029/2009JC005312, 2009.

Lemke, P. *et al.*, Observations: Changes in Snow, Ice, and Frozen Ground. In *Climate Change 2007: The Physical Science Basis. Contribution of Working Group I to the Fourth Assessment Report of the Intergovernmental Panel on Climate Change*, Solomon, S. *et al.*, Eds. (Cambridge University Press, Cambridge, United Kingdom and New York, NY, USA, 2007.

Leonard, K. C. & Maksym, T. The importance of wind-blown snow redistribution to snow accumulation on and mass balance of Bellingshausen Sea ice, *Ann. Glaciol.*, **52**(57), 2011.

Liu, J. and J. A. Curry, Accelerated warming of the Southern Ocean and its impacts on the hydrological cycle and sea ice, *Proc. Nat. Acad. Sci.*, **107**, 14987–14992, 2010.

Maksym, T. & Markus, T. Antarctic sea ice thickness and snow-to-ice conversion from atmospheric reanalysis and passive microwave snow depth, *J. Geophys. Res.*, **113**, C02S12, 2008.

Manabe, S., Spelman, M. J. & Stouffer, R. J. Transient responses of a coupled ocean-atmosphere model to gradual changes of atmospheric CO₂ part II: seasonal response, *J.*

Clim., **5**, 105, 1992.

Markus, T. & Cavalieri, D. J. An enhancement of the NASA Team sea ice algorithm, *IEEE Trans. Geosc. Rem. Sens.*, **38**(3), 1387-1398, 2000.

Markus, T. & Cavalieri, D. J. Snow depth distribution over sea ice in the Southern Ocean from satellite passive microwave data, in *Antarctic Sea Ice Physical Processes, Interactions and Variability, Antarctic Research Series*, **74**, 19-40, AGU, Washington, D.C., 1998.

Markus, T., Massom, R., Worby, A., Lytle, V., Kurtz, N., and T. Maksym, Freeboard, snow depth, and sea ice roughness in East Antarctica from in-situ and multiple satellite data, *Ann. Glaciol.*, **52**(57), 2011.

Massom, R.A., A. Worby, V. Lytle, T. Markus, I. Allison, T. Scambos, H. Enomoto, K. Tateyama, T. Haran, J.C. Comiso, A. Pfaffling, T. Tamura, A. Muto, P. Kanagaratnam, B. Giles, N. Young, G. Hyland, and E. Key, ARISE (Antarctic Remote Ice Sensing Experiment) in the East 2003: validation of satellite-derived sea-ice data products, *Annals of Glaciology*, **44**, 288-296, 2006.

Massom, R. A. *et al.*, Snow on Antarctic sea ice, *Rev. Geophys.*, **39**, 413-445, 2001.

McMinn, A, C. Ashworth, and K. Ryan, Growth and productivity of Antarctic sea ice algae under PAR and UV irradiances, *Botanica Marina*, **42**(4), pp. 401-407, 1999.

Nicolas, J. P., and D. H. Bromwich, Precipitation Changes in High Southern Latitudes from Global Reanalyses: A Cautionary Tale, *Sur. in Geophys.*, **32**(4-5), 475-494, DOI: 10.1007/s10712-011-9114-6, 2011.

Powell, D. C., Markus, T. & Stossel, A. Effects of snow depth forcing on Southern Ocean sea ice simulations, *J. Geophys. Res.*, **110**, C06001, 2005.

Rind, D., R. Healy, C. Parkinson, D. Martinson, The role of sea ice in 2 x CO₂ climate model sensitivity: Part II: hemispheric dependencies, *Geophys. Res. Lett.*, **24**, 1491-1494 (1997).

Screen, J., and I. Simmonds, 2010, The central role of diminishing sea ice in recent Arctic

temperature amplification, *Nature*, 464, 1334-1337, 2010.

Stroeve, J., Holland, M. M., Meier, W., Scambos, T. & Serreze, M. Arctic sea ice decline: Faster than forecast, *Geophys. Res. Lett.*, **34**, L09501, doi:10.1029/2007GL029703, 2007.

Wadhams, P., M. A. Lange, S. F. Ackley, The ice thickness distribution across the Atlantic sector of the Antarctic Ocean in midwinter, *J. Geophys. Res.*, **92**(C13), 14535-15,552, 1987.

Watterson, I. G. & Dix, M. R. Simulated changes due to global warming in daily precipitation means and extremes and their interpretation using the gamma distribution, *J. Geophys. Res.*, **108**(D13), 4379, doi:10.1029/2002JD002928, 2003.

Weissling, B. P., and S. F. Ackley, Antarctic sea-ice altimetry: scale and resolution effects on derived ice thickness distribution, *Ann. Glaciol.*, **52**(57) (2011).

Willatt, R. C., Giles, K. A., Laxon, S. W., Stone-Drake, L., and Worby, A. P., Field Investigations of Ku-Band Radar Penetration Into Snow Cover on Antarctic Sea Ice, *IEEE Trans. Geosc. Rem. Sens.*, **48**(1), 2010.

Worby, A. P., A. Steer, J. L. Lieser, P. Heil, D. Yi, T. Markus, I. Allison, R. A. Massom, N. Galin, J. Zwally, Regional-scale sea ice and snow thickness distributions from in situ and satellite measurements over East Antarctica during the Sea Ice Physics and Ecosystem eXperiment (SIPEX), *Deep-Sea Res. II*, **58**, 1125-1136, 2011.

Worby, A.P., C.A. Geiger, M.J. Paget, M.L. Van Woert, S.F. Ackley, and T.L. DeLiberty, Thickness distribution of Antarctic sea ice, *J. Geophys. Res.*, **113**, C05S92, doi:10/1029/2007JC004254, 2008.

Xie, H., Ackely, S. F., Yi, D., Zwally, H. J., Wagner, P., Weissling, B., Lewis, M., and K. Ye, Sea-ice thickness distribution of the Bellingshausen Sea from surface measurements and ICESat altimetry, *Deep-Sea Res. II*, **58**, 1039-1051, 2011.

Yi, D., Zwally, H. J. & Robbins, J. W. ICESat observations of seasonal and interannual variations of sea-ice freeboard and estimated thickness in the Weddell Sea, Antarctica (2003-2009), *Ann. Glaciol.*, **52**(57), 2011.

Zhang, J. Increasing Antarctic sea ice under warming atmospheric and oceanic conditions, *J. Climate*, **20**, pp. 2515-2529, 2007.

Zwally, H.J., R. Schutz, C. Bentley, J. Bufton, T. Herring, J. Minster, J. Spinhirne, and R. Thomas, 2003, GLAS/ICESat L2 Sea Ice Altimetry Data V531, October 2003 through March 2008. Boulder, CO: National Snow and Ice Data Center. Digital media.

Zwally, H. J., Comiso, J. C., Parkinson, C. L., Cavalieri, D. J. & Gloersen, P. Variability of Antarctic sea ice 1979-1998, *J. Geophys. Res.*, **107**, C5, 3041, 2002.

Zwally, H. J., Yi, D., Kwok, R. & Zhao, Y. ICESat measurements of sea ice freeboard and estimates of sea ice thickness in the Weddell Sea, *J. Geophys. Res.*, **113**, C02S15, doi:10.1029/2007JC004284, 2008.

8 Acknowledgments

The ship-based sea ice and snow thickness data used in the methods comparison were provided by the SCAR Antarctic Sea Ice Processes and Climate (ASPeCt) program (www.aspect.aq).

8.1 Figure and table captions

Figure 1: Maps of the averaged sea ice thickness data for each season from 2004-2008.

Figure 2: Distribution of sea ice thickness results for all ICESat measurements.

Figure 3: Freeboard, sea ice thickness, sea ice areal coverage (for areas with greater than 50% ice concentration), and sea ice volume averages for each ICESat campaign period.

Figure 4: Map of the different sectors referred to in the study. Longitude boundaries for the regions are 1) Ross Sea: 160° - 230° , 2) Bell/Amund Sea 160° - 230° , 3) Weddell (west) 300° - 315° , 4) Weddell (east): 315° - 20° , 5) Indian: 20° - 90° , 6) Pacific: 90° - 160° .

Table 1: ICESat data collection time periods.

Table 2: Average sea ice thickness results using ICESat data compared to geographically and temporally coincident ASPeCt ship observations.

Table 3: Trends in sea ice thickness and volume by region. Values not in parentheses are trends calculated using sea ice areal coverage equivalent to the dates from the spring 2004 campaign, while those in parentheses are calculated using the dates shown in Table 1.

9 Tables

Year	Dates		
	Spring	Summer	Fall
2003	Oct 1 to Nov 18	-	-
2004	Oct 3 to Nov 8	Feb 17 to Mar 21	May 18 to Jun 21
2005	Oct 21 to Nov 24	Feb 17 to Mar 24	May 20 to Jun 23
2006	Oct 25 to Nov 27	Feb 22 to Mar 27	May 24 to Jun 26
2007	Oct 2 to Nov 5	Mar 12 to Apr 14	-
2008	-	Feb 17 to Mar 21	-

Table 1:

	ICESat mean (m)	ASPeCt mean (m)	ICESat - ASPeCt (m)	# of grid cells
All ship observations (1981 - 2005)				
Spring (Oct. 1 - Dec. 1)	0.82	0.78	0.04	846
Summer (Feb. 1 - Apr. 1)	0.52	0.36	0.16	582
ICESat era ship observations (2003 - 2005)				
Spring	0.79	0.73	0.06	79
Summer	0.58	0.35	0.23	86

Table 2:

Sector	Total	Ross Sea	Bell/Amund Sea	Weddell (west)	Weddell (east)	Indian	West Pacific
Ice thickness trend [m/yr]	-0.03	Summer (February-March)	0.07	-0.06	-0.04	-0.11	-0.03
Ice volume trend [km ³ /yr]	160	-0.01	-30	-50	57	92	0
		88					
		Spring (October-November)					
Ice thickness trend [m/yr]	-0.02 (-0.02)	-0.01 (-0.01)	0.05 (0.05)	-0.07 (-0.07)	-0.04 (-0.04)	0.01 (0.0)	-0.05 (-0.04)
Ice volume trend [km ³ /yr]	-266 (-403)	107 (91)	-74 (-76)	-26 (-36)	-194 (-241)	-29 (-69)	-51 (-73)

Table 3:

10 Figures

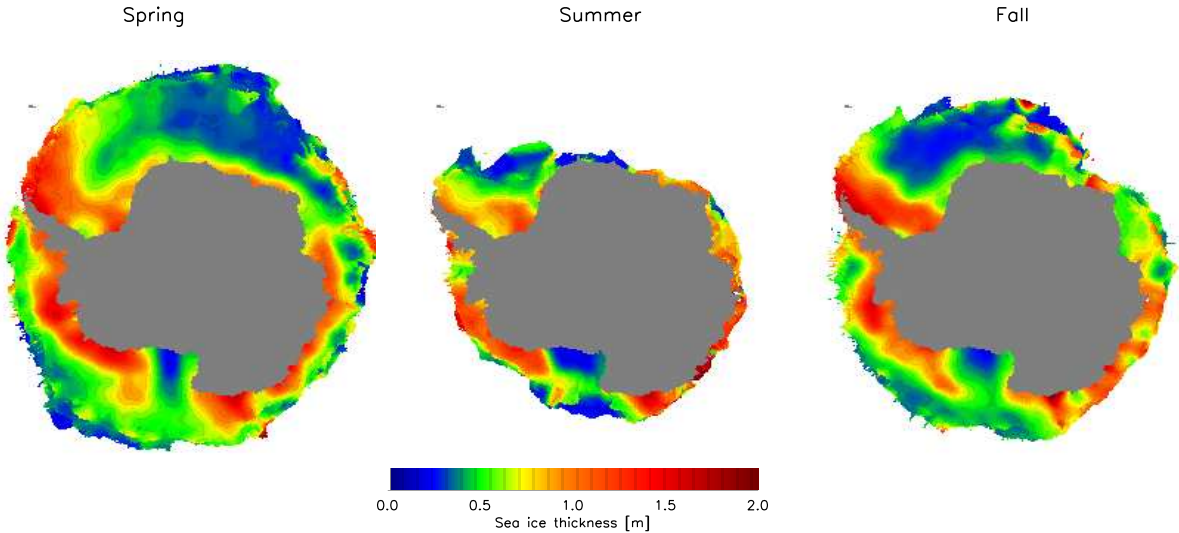


Figure 1:

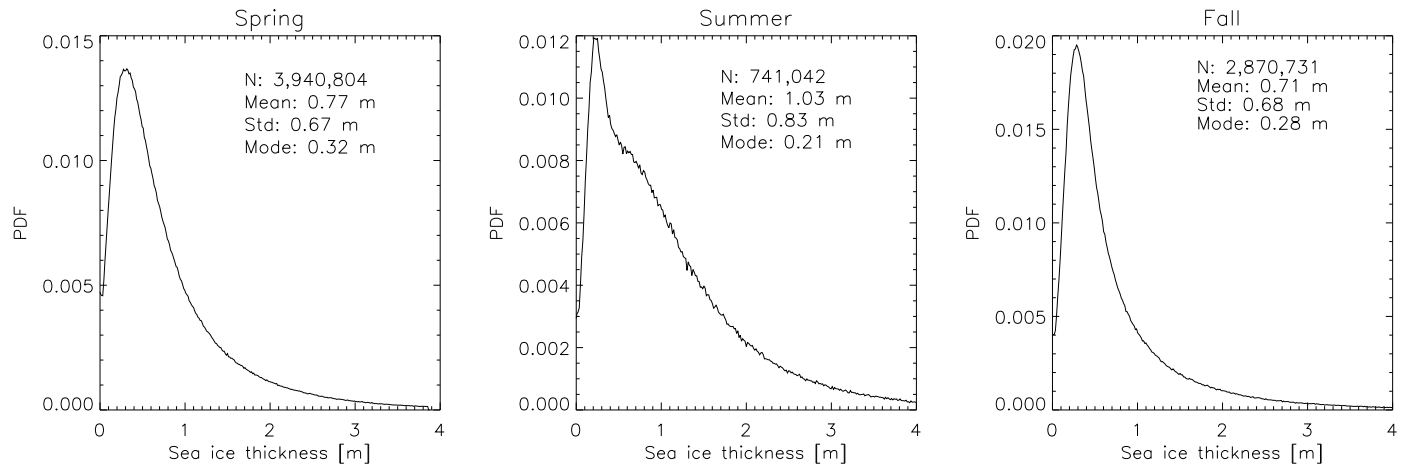


Figure 2:

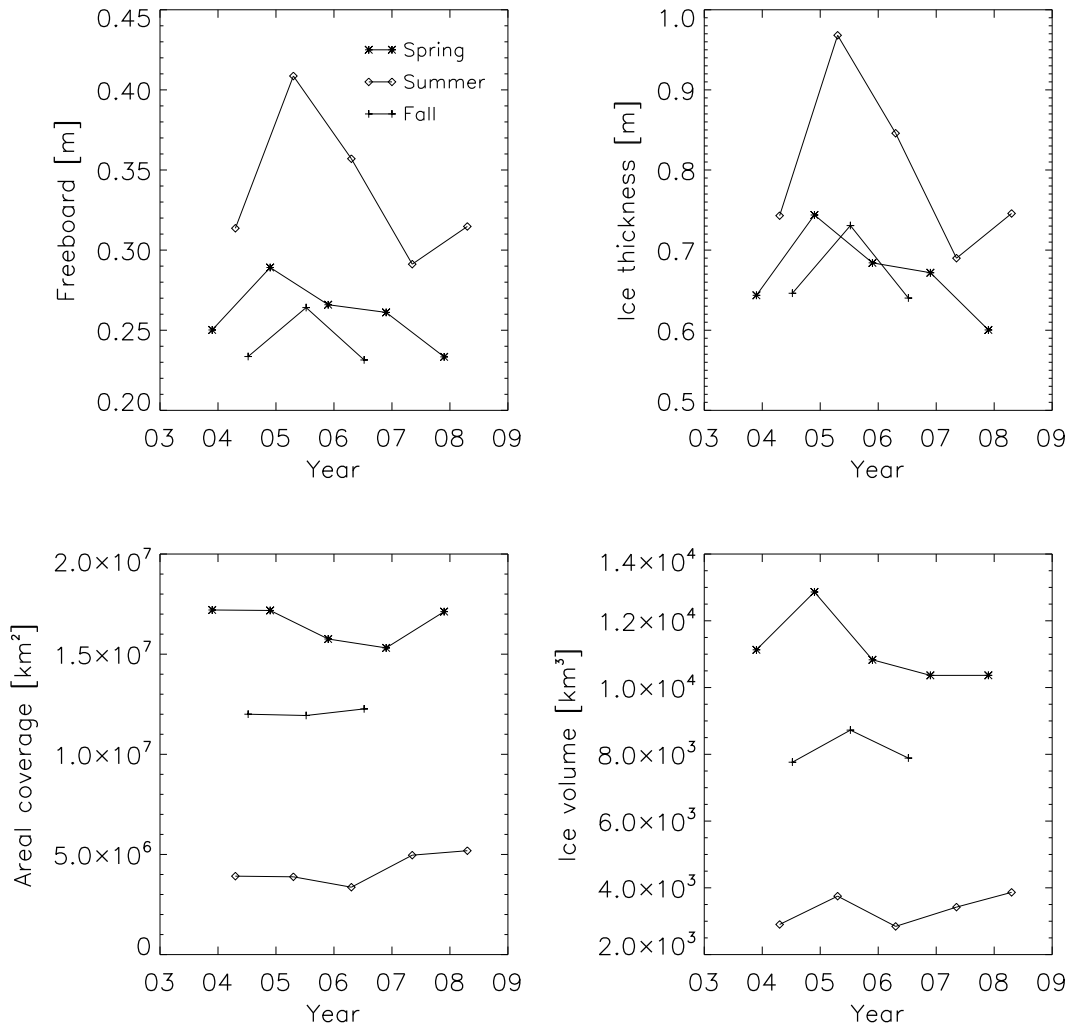


Figure 3:

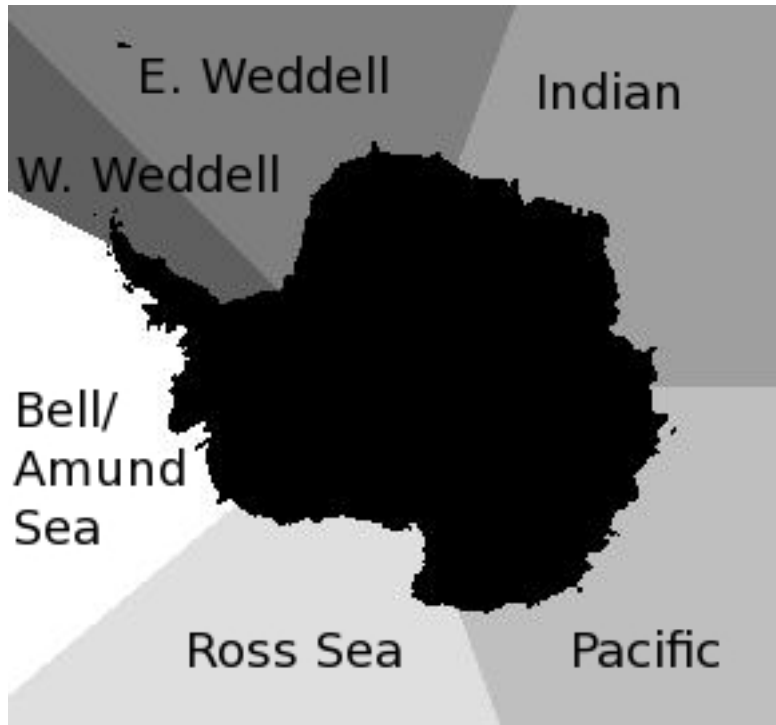


Figure 4: